SCD's Cooled and Uncooled Photo Detectors for NIR-SWIR

Rami Fraenkel, Daniel Aronov, Yael Benny, Eyal Berkowicz, Leonid Bykov, Zipi Calahorra, Tal Fishman, Avihoo Giladi, Elad Ilan, Philip Klipstein, Lidia Langof, Inna Lukomsky, David Mistele*, Udi Mizrahi, Dan Nussinson, Avi Twitto**, Michael Yassen, and Ami Zemel

SemiConductor Devices P.O. Box 2250, Haifa 31021, Israel

*** Faculty of Electrical Engineering, Technion**

**** IMOD**

ABSTRACT

Short wavelength Infra Red (SWIR) imaging has gained considerable interest in recent years. The main applications among others are: active imaging and LADAR, enhanced vision systems, low light level imaging and security surveillance systems.

In this paper we will describe SCD's considerable efforts in this spectral region, addressing several platforms:

1. Extension of the mature InSb MWIR product line operating at 80K (cut-off wavelength of 5.4µm).
2. Extension of our new $XB_n n$ InAsSb "bariode" technology operating at 150K (cut-off of 4.1µm).
3. Development of InGaAs detectors for room temperature operation (cut-off of 1.7µm)
4. Development of a SNIR ROIC with a low noise imaging mode and unique laser-pulse detection modes.

In the first section we will present our latest achievements for the cooled detectors where the SWIR region is combined with MWIR response. Preliminary results for the NIR-VIS region are presented where advanced substrate removal techniques are implemented on flip-chip hybridized focal plane arrays.

In the second part we will demonstrate our VGA, 15µm pitch, InGaAs arrays with dark current density below 1.5nA/cm^2 at 280K. The InGaAs array is hybridized to the SNIR ROIC, thus offering the capability of low SWaP systems with laser-pulse detection modes.

Keywords: SWIR, Infrared Detector, Bariode, InGaAs, XB_nn, InSb

1. INTRODUCTION AND BACKGROUND

Short wavelength Infra Red (SWIR) imaging has gained considerable interest in recent years. The main applications among others are: active imaging and LADAR, enhanced vision systems (EVS), low light level imaging and security surveillance systems.

Historically, SCD entered the SWIR region about 10 years ago via the EVS application. In this application the detector fuses a thermal image in the MWIR with landing lights in the SWIR. The traditional and mature InSb technology was extended towards 1µm utilizing the *Blue Fairy* readout[1], followed by the *Pelican* readout[2].

The next step was the introduction of the *SNIR* detector[3,4] which is a 640x512/15µm InSb detector, with a Read Out Integrated Circuit (ROIC) that incorporates a higher level of signal processing. The 0.18µm CMOS process allows in-pixel high functionality, and at a relatively low level of power consumption. Specifically, it incorporated a low noise readout mode (LNIM) which is suitable for both active and passive imaging in the SWIR.

Over the last few years SCD has been developing a new type of patented MWIR detector known as a "bariode" or XB_nn detector[5,6]. This detector can perform at an elevated temperature of 150K thus providing a great advantage for low SWaP systems. The XB_nn layers are grown on GaSb substrates and since GaSb has a bandgap wavelength at 150K of ~1.6µm, it determines the cut-on wavelength. With the removal of the substrate the detector exhibits a significant response at

shorter wavelengths, only vanishing at a wavelength of about 0.5μm. The total removal of the GaSb substrate by selective etching is therefore an essential first step in opening the detector response to the SWIR wavelength range. The combination of XB_nn technology and the SNIR ROIC is highly desirable for further power reduction and compactness.
Among the available technologies with the capability to detect wavelengths from visible to SWIR, InGaAs grown on an InP substrate appears to be an excellent candidate[7]. Unlike InSb or XB_nn it can be operated close to room temperature with obvious advantages. The development of InGaAs detectors was launched at SCD in 2010 in the framework of the *HYSP* (Hyper Sensitive Photonics) consortium. The main goal is to address low light level (LLL) applications. The first demonstrator was introduced in 2011: A VGA 15μm pitch InGaAs array was hybridized to the SNIR ROIC utilizing its special active and passive features. We have achieved dark current densities lower than 1.5 nA/cm^2 at 280K. This demonstrator is currently being developed to a full product.

The paper is organized as follows: In the first part we present the cooled technology, namely InSb and XB_nn InAsSb. (The SNIR ROIC performance is beyond the scope of this article and was described extensively elsewhere[3]). In order to determine the factors that limit the SWIR and especially the VIS response we have developed a theoretical photo-detector model that will be elaborated.

In the second part we will review the performance of the InGaAs demonstrator utilizing the low noise high gain (LNIM) mode of the SNIR ROIC. We will also exhibit preliminary results for the NIR-VIS response following substrate removal and some active mode (ALPD and TLRF) results.

2. SWIR RESPONSE OF InSb and XB_nn InAsSb DETECTORS

The need for "opening" the InSb arrays to the SWIR region arose from the EVS application. The EVS system facilitates aircraft precision approach and safe landing in reduced visibility conditions, including thick fog, smog, heavy rain and snow. EVS's operating bandwidth fuses both the short and medium IR spectrum to provide clear images of approach and runway lights, runway threshold, buildings, other visual cues, obstructions and aircraft in close proximity. These images normally are undetectable to the pilot's naked eye at night and in bad weather. For this purpose the InSb FPA backside process was optimized to support a cut on wavelength down to 1.3μm. Recent landing regulations now require an extension to the visible range, namely down to 600nm (0.6μm). However, with the existing process the FPAs could not be operated below 1.1μm due to "latent" image effects. The backside process was modified in order to reduce this effect. Figure 1 shows the spectral response of a *Pelican* FPA with an extended response into the NIR and Visible range, measured by a monochromator spectrometer. .

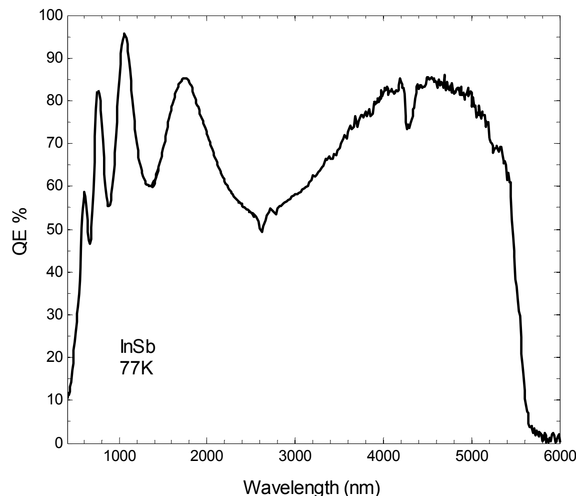

Figure 1: Spectral Response of a *Pelican* (640x512/15μm) FPA with improved backside process extending to the VIS-NIR.

Over the last few years SCD has been developing a new type of patented MWIR detector known as an XB_nn *bariode* detector[5,6]. A *bariode* is a new type of semiconductor device, in which the transport of majority carriers is blocked by a barrier in the depletion layer, while minority carriers, created thermally or by the absorption of light, are allowed to pass freely across the device[11]. In an *n*-type bariode, also known as an XB_nn device, the active photon absorbing and barrier layers are doped with electron donors, while in a *p*-type bariode, or XB_pp device, they are doped with electron acceptors. An important advantage of bariode devices is that their dark current is essentially diffusion limited, so that very high detector operating temperatures can be achieved[10].

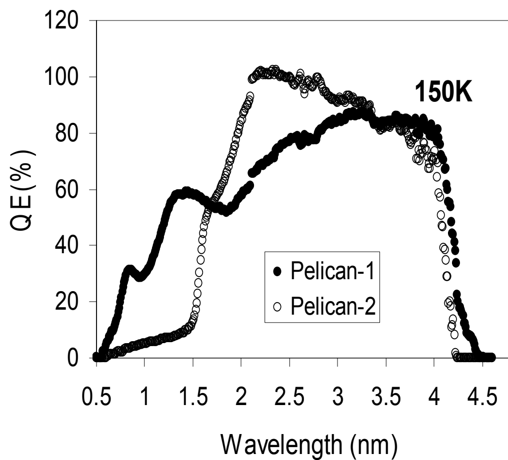

Figure 2:
Spectral response, averaged over all pixels, for two 15μm pitch, 640×512, detectors bonded to SCDs *Pelican* ROIC. In FPA Pelican-1, the GaSb substrate has been totally removed while in Pelican-2, several microns remain.

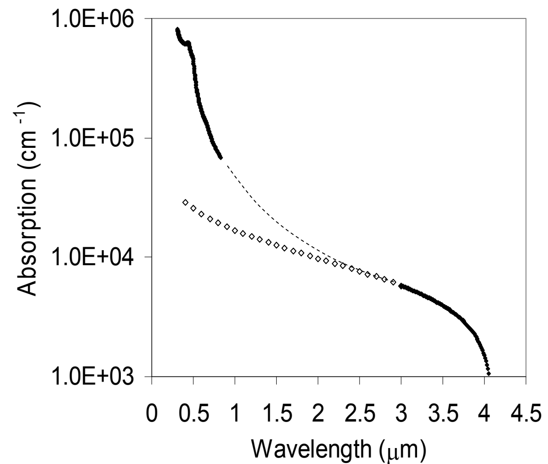

Figure 3:
Absorption coefficient spectrum of $InAs_{1-x}Sb_x$ alloy with x~0.09. Solid points on right hand side and open symbols: absorption calculated from the phenomenological model of Ref. 10. *Solid points on left hand side*: absorption data from Aspnes and Studna[9]. *Dashed line*: guide for the eye.

Figure 2 shows the spectral photoresponse at 150K of two n-type bariode detector arrays with a 15μm pitch bonded to SCD's *Pelican* ROIC. In both cases the active layer is an $InAs_{1-x}Sb_x$ alloy with x~0.09 and a thickness of t_{AL}=3μm. During MBE growth, the active layer is separated from the GaSb substrate by an n^+ InAsSb buffer layer 0.5μm thick. In the case of FPA Pelican-1, the GaSb substrate was totally removed during processing using a selective etch, while in FPA Pelican-2, several microns of GaSb remained after removal of the rest of the substrate by chemical-mechanical polishing. Since GaSb has a bandgap wavelength at 150K of ~1.6μm, the remains of the GaSb substrate determine the cut-on wavelength in Pelican-2. In contrast Pelican-1, with no remainder of GaSb, exhibits a significant response at shorter wavelengths, only vanishing at a wavelength of about 0.5μm. The total removal of the GaSb substrate by selective etching is therefore an essential first step in opening the detector response to the NIR-SWIR wavelength range.

In order to determine the factors that limit the SWIR response we have developed a theoretical photo-detector model in which we have added to the optical transfer matrix model that we have reported previously[8] the effects of:

(i) surface recombination at the interface between the n^+ InAsSb buffer layer and a dielectric antireflection coating at the back of the FPA. The surface recombination is characterized by a parameter D/s where D is the minority carrier diffusion coefficient in the buffer and s is the surface recombination velocity;

(ii) the diffusion of the photo-created carriers to the active layer, with diffusion length, L_{Buf} ;

(iii) the diffusion of the photo-created carriers across the active layer, with diffusion length, L_{AL};

Full details of our model will be presented elsewhere[14].

Figure 3 shows the absorption coefficient of nominally undoped $InAs_{0.91}Sb_{0.09}$ alloy. The solid points at wavelengths (λ) greater than 3μm are calculated from the phenomenological model we have reported previously for the alloy, and tested successfully against many of our InAsSb XB_nn detectors at wavelengths greater than 3μm[8, 10]. The open points are an extrapolation of the phenomenological model to wavelengths shorter than 3μm. Below $\lambda \approx 2$μm, this model starts to underestimate the true value of the absorption coefficient quite significantly. The solid points at wavelengths shorter than 0.82μm are those calculated from a weighted average of the data reported by Aspnes and Studna for InSb and InAs, based on spectroscopic ellipsometry measurements[9]. We have no reliable data for the region in between 0.82μm and 3μm, which is therefore sketched as a dashed line, only as a guide for the eye.

The first point to note from the short wavelength data in Figure 3 is that at a wavelength of ~0.5 μm, the absorption coefficient is very large: $\alpha = 4.38\times10^5$ cm^{-1}, and this corresponds to an absorption length of only ~ 200Å. It means that in this wavelength region, virtually all of the light is absorbed in the buffer layer, very close to its back surface. Most of the photo-created minority carriers are therefore likely to be lost by surface recombination or by recombination in the buffer layer, where the diffusion length is quite short. This is why the QE at λ ~ 0.5 μm is very low. In order to increase the QE the thickness of the buffer layer and/or the surface recombination velocity need to be reduced. These effects are shown in Figure 4 and Figure 5, where we have used our new detector model to simulate the QE.

In Figure 4, the measured spectrum of Pelican-1 shown in Figure 2 is reproduced as a doted line. The thin solid line that extends to ~4.2 μm is the QE calculated with our model using the phenomenological formula for the absorption coefficient over the whole wavelength range. As mentioned above, this model tends to deviate from the real absorption coefficient for λ<2μm, and the simulation in Figure 4 shows that, with this absorption coefficient, our model overestimates the measured QE quite significantly at short wavelengths. On the other hand, when we insert the absorption data of Aspnes and Studna, measured over the range $0.5<\lambda<0.82$ μm, the agreement of our model with the measured QE becomes quite good (thick dashed line). In order to get good agreement we found fitted values: D/s=0.01 μm and L_{Buf} = 0.5μm. These same values were also used over the whole wavelength range in the spectrum that was calculated from the phenomenological model. The short diffusion length is related to the high doping in the buffer layer, as discussed in Ref. 10.

We use our model in Figure 5 to demonstrate the effect of the main buffer parameters on the QE at short wavelengths. In all cases the active layer thickness and diffusion length were t_{AL}=3μm and L_{AL}=50μm, respectively. The latter figure is based on estimates we reported earlier for the diffusion length in the low doped InAsSb active layer of our detector structures[10]. In Figure 5 (a) we demonstrate the effect of the surface recombination velocity. This Figure shows that for D/s ≤ 0.01μm, the spectral dependence of the QE becomes very insensitive to the surface recombination velocity, and that our detector structure, Pelican-1, is already in this regime of high surface recombination velocity i.e. nearly all of the holes created in the buffer layer are removed by recombination at the back surface. If the surface recombination velocity can be reduced by two orders of magnitude so that D/s ≈ 1 μm, then it is possible to achieve a QE in excess of 40% for a 0.5 μm thick buffer layer with a diffusion length of ~0.5 μm. In Figure 5 (b), we show how the QE increases rapidly as the buffer thickness is reduced for D/s = 0.01μm and a buffer diffusion length of 0.5 μm. The QE at ~0.55 μm exceeds 40% when the buffer thickness is reduced to ~ 0.1 μm. Finally in Figure 5 (c), we examine the effect of the buffer diffusion length for D/s = 0.01μm and a buffer thickness of 0.5 μm. Not surprisingly, when the diffusion length in the buffer exceeds the buffer thickness, the QE becomes insensitive to its exact value, whereas when the diffusion length becomes much less than the buffer thickness, the QE rises slowly from a very low value and represents the situation where all the minority carriers created in the buffer do not escape. In this limit, the buffer simply acts as an optical filter.

Based on the trends discussed above, we can deduce that in our detectors in which the GaSb substrate has been totally removed, D/s ≈ 0.01μm and $L_{\mathrm{Buf}} \approx 0.5$ μm, because these values result in a reasonably good fit to our measured spectral response in a device where the buffer layer thickness is $t_{\mathrm{Buf}} \approx 0.5$ μm.

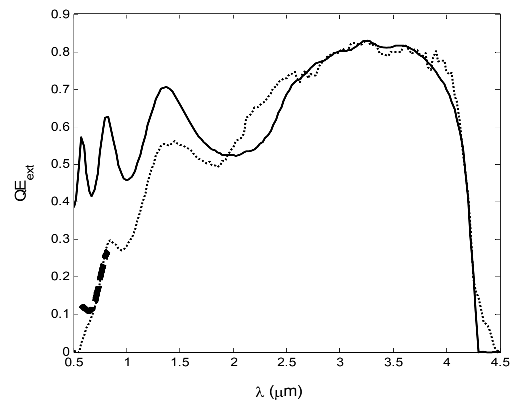

Figure 4
*Solid lines***:** Simulated spectral response using the detector model described in the text, in which we have used either the phenomenological absorption spectrum of Ref. 10 (thin, solid) or the absorption spectrum of Aspnes and Studna[9] (thick, dashed) and parameter values: D/s=0.01μm, $L_{\mathrm{Buf}} = t_{\mathrm{Buf}} = 0.5$μm. *Dotted line*: Measured spectrum of FPA Pelican-1, shown in Figure 2.

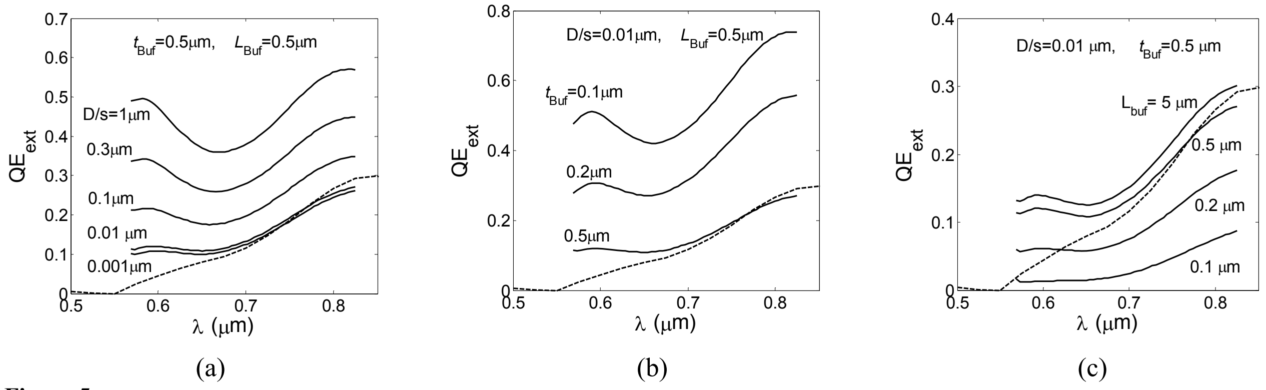

(a) (b) (c)

Figure 5
Simulated behaviour of FPA detector with active layer thickness and diffusion length of t_{AL}=3µm, L_{AL}=50µm, respectively. In (a) the surface recombination velocity is varied, in (b) the buffer thickness is varied and in (c) the buffer diffusion length is varied.

In Figure 6, we show the behaviour expected for a more optimized device with a thinner buffer layer of 0.2 µm. This simulation shows that the short wavelength QE will be relatively insensitive to the diffusion length and hence to the buffer doping. For this buffer layer thickness, QE>30% looks quite feasible at λ > 0.6 µm. Figure 5 (b) shows that it is necessary to reduce the buffer layer thickness below 0.1 µm in order to achieve QE > 40% for λ > 0.5 µm. Further short wavelength sensitivity can be achieved only by reducing the surface recombination velocity.

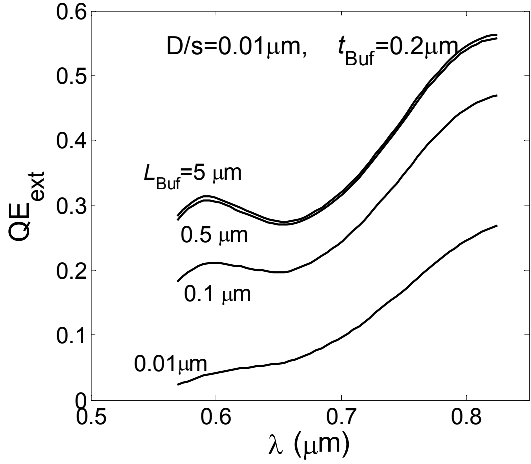

Figure 6
Simulated spectral response for the same detector as in Figure 5 with D/s=0.01 µm and buffer thickness, t_{Buf}, of 0.2 µm.

3. InGaAs DETECTORS FOR LOW LIGHT LEVEL APPLICATIONS

The development of InGaAs detectors was launched at SCD in 2010 in the framework of the *HYSP* (Hyper Sensitive Photonics) consortium. The main goal of the consortium is to address low light level (LLL) applications utilizing InGaAs detectors for the SWIR region where we can benefit from the contribution of the "Night Glow"[12]. The first FPA demonstrator was introduced in 2011: a 640x512 15µm pitch InGaAs array was hybridized to the SNIR ROIC[3] utilizing its low noise high gain (LNIM) mode and the special laser detection active modes. Currently we are designing an optimized product based on this FPA. It consists of a low SWaP package and low power proximity electronics.

In the following sections we will elaborate on the FPA process and electro-optical characterization results. Special attention will be devoted to the performance in the LNIM mode. Preliminary measurement results of the active modes (ALPD and TLRF) will be discussed as well.

3.1 InGaAs Array

The sensing array consists of a typical PIN InGaAs on InP heterostructure grown by the MOCVD method. The p+ junctions are created by diffusion through InP windows. The passivation layers ensure high stability and reliability. The structure was optimized with the aid of test structures and simulation tools achieving the proper trade-off between responsivity, dark current and pixel to pixel cross-talk. This is shown in Figure 7 where we exhibit an FPA divided into small blocks. Each block contains a different combination of pixel design and the dark current, dynamic resistance and QE can be measured collectively.

The arrays are hybridized to the SNIR ROIC. The baseline is SCD's mature 15µm pitch Indium bump process that was originally developed for the *Pelican* and *Pelican-D* detectors[2]. Some modifications of the transition metals and hybridization parameters were needed and implemented accordingly.

Backside illuminated InGaAs detectors are sensitive in the 0.9µm to 1.7µm region where the cut on is imposed by the InP substrate. We have developed a combined mechanical and chemical thinning process of the InP substrate thus opening the detector to the NIR and VIS region. Figure 8 exhibits the relative spectral response of a thinned detector with and without AR coating. A QE of 75% was measured facing a uniform illumination from an integrating sphere at 1550 nm.

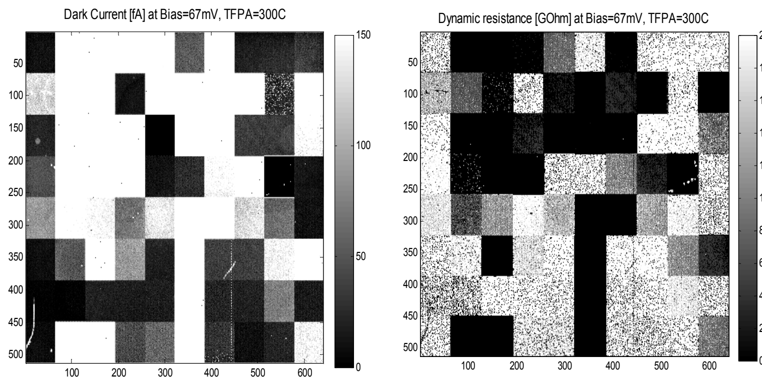

Figure 7
A test structure consisting of FPA divided into small blocks

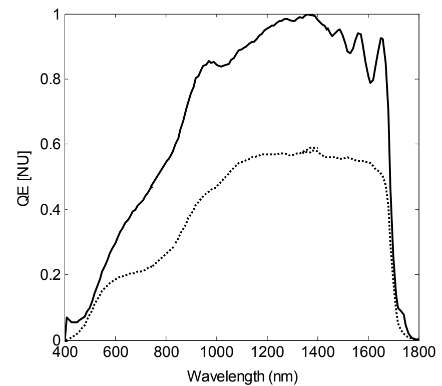

Figure 8
Relative spectral response of a thinned wafer with and without AR coating.

3.2 Dark Current

The dark current is a critical figure of merit for low light level applications. If the current is too high it will overwhelm the readout "floor noise" especially for longer integration periods. It can be reduced by cooling but this requires excess power consumption undermining demands for "low SWaP". Figure 9 presents a typical dark current histogram for a reverse bias of 100mV. At ambient temperature the mean value is 40fA with a FWHM of less than 10fA. In Figure 10 we show the variation of the dark current with FPA temperature indicating that it is governed by a diffusion mechanism in the InGaAs absorption material [13].

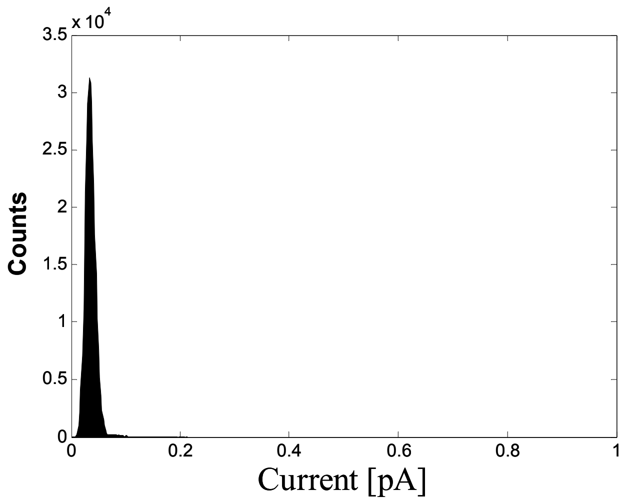

Figure 9
Typical dark current distribution at ambient temperature

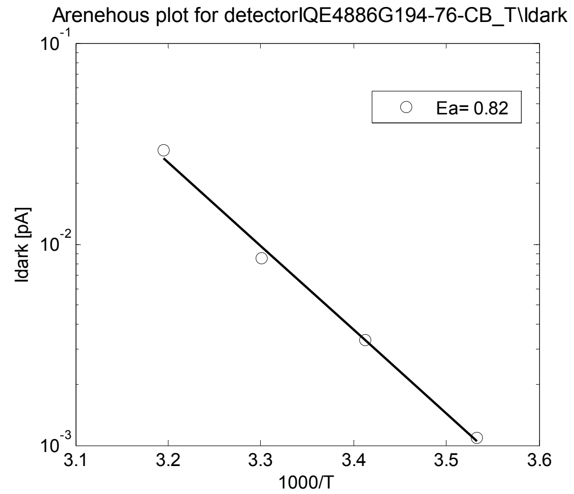

Figure 10
Dark current vs. FPA temperature indicating a diffusion mechanism.

3.3 LNIM mode

The LNIM mode is a low noise, high gain mode designed for low light level imaging applications. It can be used in passive imaging with a long integration period, or in active imaging with a very short integration time. The integration time in LNIM active mode can be lower than 30 µsec. For passive imaging the dark current should be considerably lower than the photo current and floor noise. By cooling the FPA to 280K we can reduce the dark currents well below 10fA.
First we present the electro-optical performance of the passive (long integration time) LNIM mode. All measurements were performed using an F/2 aperture while facing 1.5 µm, uniform illumination, at the output of an Integrating Sphere. For best performance we use pixel Correlated Double Sampling (CDS). In the SWIR spectral range the Noise Equivalent Power (NEP) is the key parameter which is used to define the sensitivity. A typical NEP histogram for a 10msec integration period is shown in Figure 11. NEP median value is ~ 0.6fW with a FWHM of ~ 0.2fW.

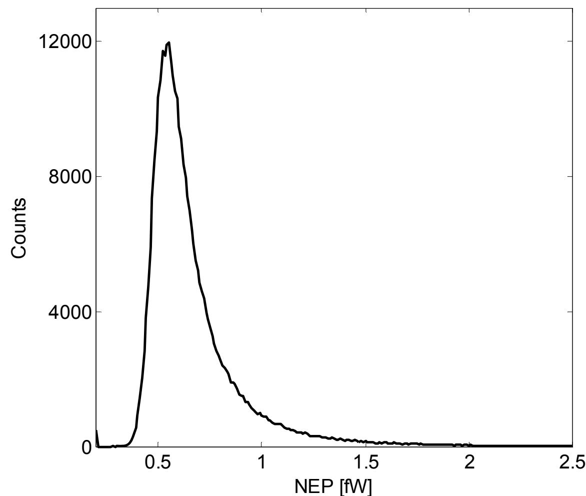

Figure 11 LNIM typical NEP histogram for 10msec integration period.

In Figure 12 we show the RNU of the LNIM after 2 point correction and a linear fit correction, as a function of well fill capacity measured at different integration periods and constant flux. Each point is an average of 64 consecutive frames. The RNU is presented in units of STD over full dynamic range. The RNU after linear fit correction in the LNIM mode is less than 0.1% STD/full range for signals between 10-60% well-fill capacities. For reference we present the corrected image for 40% well fill, which shows "white spatial noise".

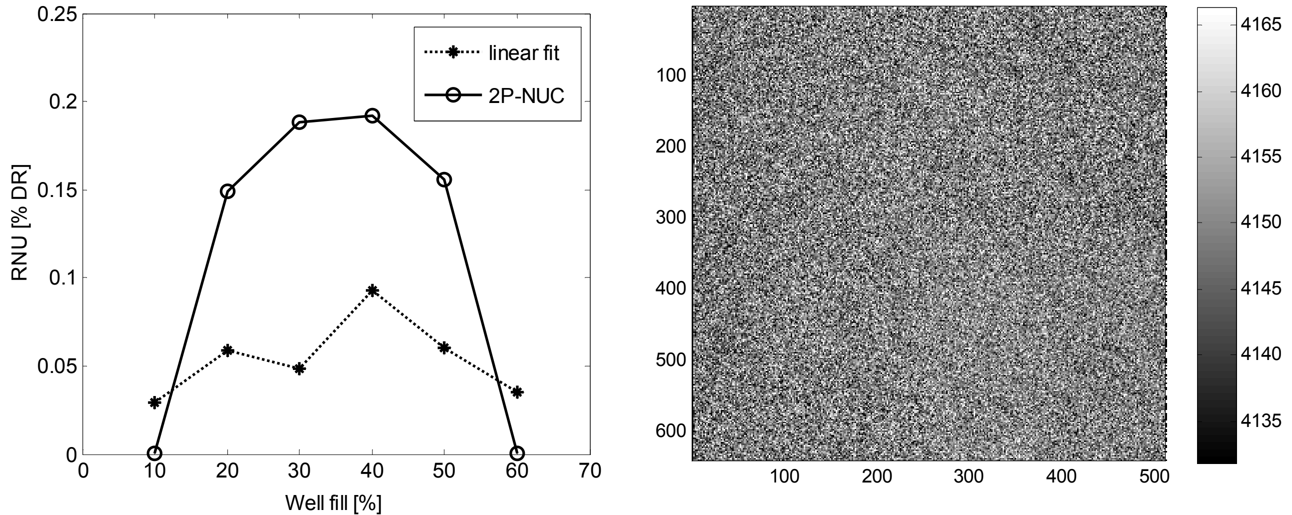

Figure 12
LNIM RNU after 2 point and linear fit correction and corrected image at 40% well fill.

3.4 Active modes: ALPD and TLRF

The two main active modes ALPD and TLRF were discussed thoroughly elsewhere[3,4]. Here we present preliminary data for the InGaAs FPA at room temperature. In the ALPD mode we define new parameters which are important for the ALPD characterization: False Alarm Rate (FAR) per pixel as the percentage of frames indicating false laser pulse detection for a specific pixel, mean array FAR as an average FAR of all non-defective pixels, and Detectivity as the percentage of frames indicating true laser detection for a specific pixel. There are two kinds of defects defined in the ALPD mode: FAR defects - pixels with FAR above a certain threshold value (e.g. 20%), and Detectivity defect - pixels with Detectivity which is less than a certain threshold value (e.g. 80%). We also define Operability as the percent of pixels, out of all matrix pixels, that have Detectivity greater than 80% and are not FAR defects. Figure 13 shows the Operability measured as a function of laser power (in electrons per pixel) for different Detectivity thresholds. For a sensitivity of 150 e/pixel, an operability higher than 95% is achieved.
The measurement setup for the TLRF mode includes pulsed laser, pulse generator, laser attenuator, beam splitter, fast diode for laser pulse monitoring, and imaging optics. The pulse generator is triggered by a Frame Start pulse coming from the detector. It generates the signal at a given delay and with a controlled pulse width. This signal is used to drive the 1.5 μm diode pulsed laser. The laser signal was characterized by the LNIM active mode at every pixel, and the amplitude was controlled by the attenuator. Time of flight was measured by varying the laser pulse delay to imitate a real distance. The time span was varied in discrete steps between 3 to 120 μsec. In the TLRF mode, FAR, Detectivity, Operability, and FAR and Detectivity defects are defined in the same manner as in the ALPD mode. In Figure 14 we exhibit the TLRF Operability as a function of laser power for different time spans.

Although preliminary, these results seem promising for low SWaP eye-safe laser applications. Further work is needed in order to establish the various thresholds and constraints.

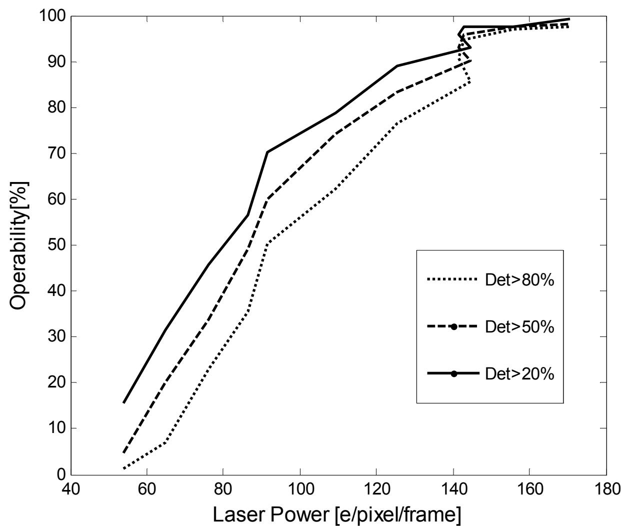

Figure 13

ALPD Operability vs. Laser Power

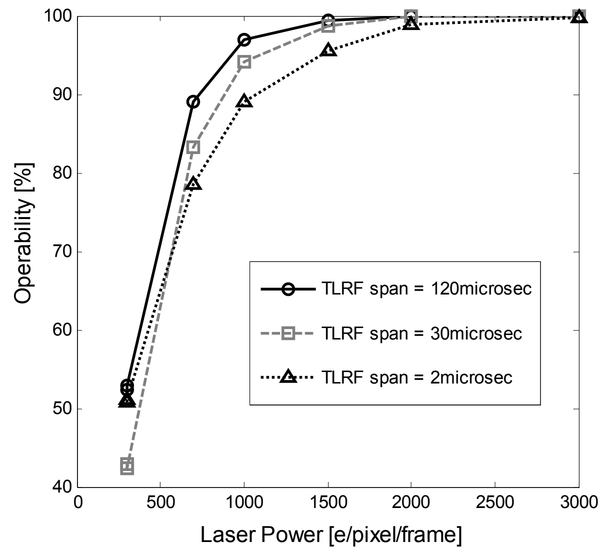

Figure 14

TLRF Operability vs. Laser Power

4. SUMMARY AND CONCLUSIONS

In this paper we have presented SCD's extensive activity in the Short Wave (SWIR) and Near (NIR) Infra-red regime. In the first part we described the cooled detectors where the SWIR region is superimposed on the standard MWIR imaging region. This applies to both planar InSb and the new XB_nn InAsSb technology. We have also presented a photo-detector model that explains the NIR-VIS response.

The second part summarizes the recent development of an InGaAs FPA based on the SNIR ROIC. We have presented promising results for Low Light Level (LLL) conditions utilizing the high gain low noise (LNIM) mode as well as initial measurements with SNIR's active modes: ALPD and TLRF. Currently we are developing a full product which will consist of the existing FPA incorporated with a low SWaP package and proximity electronics.

ACKNOWLEDGMENTS

This work was supported by the Israeli Ministry of Industry, Trade and Labor (MOITAL) and the Israeli Ministry of Defense (IMoD). We are in debt to the numerous engineers and technicians participating in the project, for their dedicated contribution to the development and production of the detectors. Specifically, we would like to acknowledge the support of the InGaAs activity provided by Hyper Sensitive Photonics (HYSP) consortium.

REFERENCES

[1] O. Nesher and P. Klipstein, "High performance IR detectors at SCD present and future", Proceedings of SPIE vol. 5957, Infrared Photoelectronics, August. 2005, pp 0S1-OS12.

[2] J. Oiknine Schlesinger, Z. Calahorra, E. Uri, O. Shick, T. Fishman, I. Shtrichman, E. Sinbar, V. Nahum, E. Kahanov, B. Shlomovich, S. Hasson, N. Fishler, D. Chen, T. Markovitz, " Pelican – SCD's 640×512/15 μm pitch InSb detector" Proceedings of SPIE vol. 6542, Infrared Technology and Applications XXXIII Conference, July. 2007, pp 654231-1-8

[3] Lidia Langof, Dan Nussinson, Elad Ilan, Shimon Elkind, Roman Dobromislin, Itzik Nevo, Fanny Khinich, Michael Labilov, Zipora Calahorra, Shay Vaserman, Tuvy Markovitz, Ofer Manela, David Elooz, Avi Tuito, Dov Oster, " Advanced multi-function infrared detector with on-chip processing" Proceedings of SPIE vol. 8012, Infrared Technology and Applications XXXVII Conference, April 2011, pp 80120F-80120F-13

[4] Lidia Langof, Dan Nussinson, Elad Ilan, Shimon Elkind, Roman Dobromislin, Itzik Nevo, Fanny Khinich, Michael Labilov, Zipora Calahorra, Shay Vaserman, Tuvy Markovitz, Avi Tuito, Dov Oster, " Multi-function IR detector with on-chip signal processing" OPTRO 2012, February 2012.
[5] P.C. Klipstein, *Depletionless Photodiode with Suppressed Dark Current*…, US Patent 7,795,640 (2 July 2003).
[6] P.C. Klipstein, *Unipolar semiconductor photodetector with Suppressed Dark Current*…, US Patent 8,004,012 (6 April 2006)
[7] A. Rouvie et al. " Low noise and low dark current 640x512 InGaAs module for low light level imaging" OPTRO 2012, February 2012.
[8] P.C. Klipstein, O. Klin, S. Grossman, N. Snapi, B. Yaakobovitz, M. Brumer, I. Lukomsky, D. Aronov, M. Yassen, B. Yofis, A. Glozman, T. Fishman, E. Berkowicz, O. Magen, I. Shtrichman, and Eliezer Weiss, "*XBn Barrier Detectors for High Operating Temperatures*", Proc. Quantum Sensing and Nanophotonics Devices VII, SPIE **7608**, 7608-1V (2010).
[9] D.E. Aspnes and A.A. Studna, "*Dielectric functions and optical parameters of Si, Ge, GaP, GaAs, GaSb, InP, InAs, and InSb from 1.5 to 6.0 eV*" Phys. Rev. B **27**, 985 (1983).
[10] Philip Klipstein, Olga Klin, Steve Grossman, Noam Snapi, Inna Lukomsky, Michael Yassen, Daniel Aronov, Eyal Berkowitz, Alex Glozman, Tal Fishman, Osnat Magen, Itay Shtrichman, and Eliezer Weiss, "*XBn barrier Photodetectors based on InAsSb with high operating temperatures*", Journal of Optical Engineering **50**, 061002 (2011).
[11] P.C. Klipstein, XBn Barrier Photodetectors for High Sensitivity and High Operating Temperature Infrared Sensors, Proc. SPIE 6940, 6940-2U (2008).
[12] Midavaine et al. "Solid state low light level imaging from UV to IR, needs and solutions", Proc OPTRO 2010.
[13] Ami Zemel, Udi Mizrahi, Tal Fishman " Nondestructive measurement of the minority carrier diffusion length in InP/InGaAs/InP double heterostructures" Submitted to the Journal of Applied Physics 2012.
[14] P C Klipstein, to be published (2012)